# Full-PIC Code Validation and Comparison against Fluid Models on Plasma Plume Expansions

## IEPC-2017-230

*Presented at the 35th International Electric Propulsion Conference*
*Georgia Institute of Technology • Atlanta, Georgia • USA*
*October 8 – 12, 2017*

Min Li[1]
*School of Astronautics, Beihang University, Beijing, 100083, P.R. China*

Mario Merino[2], Eduardo Ahedo[3]
*Equipo de Propulsión Espacial y Plasmas (EP2), Universidad Carlos III de Madrid, Leganés, 28911, Spain*

Junxue Ren[4]
*School of Astronautics, Beihang University, Beijing, 100083, P.R. China*

*and*

Haibin Tang[5]
*School of Space and Environment, Beihang University, Beijing, 100083, P.R. China*

**Abstract: An electrostatic, full-PIC code is used to study the expansion into vacuum of a 2D plasma plume. The paper first discusses the proper choice of boundary conditions for the particles and electric potential in the simulation domain to avoid or mitigate numerical artifacts. The PIC code is then used to investigate the transition from unmagnetized electrons, as in the plume of a gridded ion thruster, to magnetized electrons, as in a magnetic nozzle. The fluid codes EASYPLUME and DIMAGNO are used to benchmark and validate the PIC results in the fully-unmagnetized and fully-magnetized-electrons limits, respectively. For each simulation case, the steady state is globally achieved with the PIC code and the plasma density as well as ambipolar electric field is discussed as a function of the initial ion Mach number and initial plume divergence angle. Finally, we comment on the collisionless electron cooling mechanisms that take place in the plasma plume, and correlate these results with those of the AKILES kinetic code.**

## Nomenclature

| | | |
|---|---|---|
| $B$ | = | magnetic field strength |
| $c_s$ | = | ion sonic velocity |
| $e$ | = | unit charge |
| $J$ | = | plasma current |
| $k_B$ | = | Boltzmann constant |
| $k_M$ | = | Mach line slope |
| $M$ | = | Mach number |

[1] PhD student, School of Astronautics, lm@buaa.edu.cn
[2] Assistant Professor, Aerospace Engineering department, mario.merino@uc3m.es
[3] Professor, Aerospace Engineering department, eduardo.ahedo@uc3m.es
[4] Associate Professor, School of Astronautics, rjx_buaa@sina.com
[5] Professor, School of Space and Environment, thb@buaa.edu.cn

| | | |
|---|---|---|
| $m$ | = | particle mass |
| $n$ | = | particle number density |
| $q$ | = | electric charge quantity of a particle |
| $R_c$ | = | solenoid radius |
| $R_p$ | = | plasma radius |
| $r$ | = | radial coordinate |
| $S$ | = | particle shape factor |
| $T$ | = | thermal temperature |
| $t$ | = | simulation time |
| $v$ | = | velocity |
| $v_t$ | = | thermal velocity |
| $w_p$ | = | macro-particle weight |
| $x$ | = | length |
| $z$ | = | axial coordinate |
| $\alpha$ | = | plume divergence angle |
| $\gamma$ | = | effective cooling rate |
| $\Delta t$ | = | simulation time step |
| $\Delta x$ | = | simulation space step |
| $\theta$ | = | Mach angle |
| $\lambda_{De}$ | = | Debye length |
| $\Phi$ | = | electric potential |
| $\Omega_{\mathrm{i}}$ | = | ion gyromagnetic frequency |
| $\omega_{ce}$ | = | electron gyromagnetic frequency |
| $\omega_{pe}$ | = | electrostatic oscillation frequency |

## I. Introduction

Advanced space plasma propulsion has shown great potential advantages in application on modern satellites. Characterizing the energetic plume created by a plasma thruster is of interest for both thruster designers and system integrators, as its expansion acceleration and divergence, and its interactions with the rest of the spacecraft affects thruster performances and spacecraft integrity[1]. Physically, the process of a plasma expansion also plays an important role in other applications spanning material processing for semiconductors[2] up to astrophysical phenomena[3]. The underlying mechanisms of fundamental importance have been actively studied over the years [4-8], like the trapped electron population, electron cooling and transport, and ion acceleration via an ambipolar electric field; nevertheless, most of them are still not well understood and hence remain worthy of further research attention. Currently, as computing power increases, more complex numerical options are provided based on both fluid and kinetic approaches to predict the plasma physical properties under various magnetic circumstances during the plume expansion[9, 10]. For instance, by applying a controlled mirror-like magnetic field, the generally unmagnetized expansion process shall be complicated into the magnetized plasma confinement and steering issue[10, 11], which is favorable to propulsive performance while demands more specific illustration on the magneto-thermal-dynamic effects.

The plasma plume expansion regarding the electric propulsive applications can be conceptually divided into two distinct regions[12]. Within the so-called near-thrust region, typically a few thruster radii away from the exhaust plane, a lot of complex plasma phenomena are going on collisionally and 3D-inhomogeneously, originating from the large neutral and charged particle densities, notable residual electric and magnetic fields of the thruster, as well as presence of an external neutralizer. Thereafter in the far-thruster collisionless regime where initial inhomogeneities have died out, plasma properties seem friendly to model and simulation study. In an unmagnetized plume, the far region expansion hinges on the balance between residual electron pressure, the ambipolar electric field, and the inertia of ions; whereas in a magnetized plume, a transition to unmagnetized ions (first) and unmagnetized electrons (much farther downstream) occurs. Appropriate detachment processes of charged particles from an imposed magnetic environment allow the beam to retain converted kinetic energy from its initial thermal energy, thus to contribute to thruster performance [10, 13]. Otherwise the magnetically induced back flow would lead to propulsive momentum loss. There are two main parameters pertinent to such far-region expansion, i.e. ion Mach number and initial divergence angle, which in particular, the Mach number denotes the ratio of beam energy to electron thermal energy while the electron thermal pressure mostly drives the plume diverging rate based on the initial angle.

Indeed, such collionless plasma expansion under the fully-unmagnetized or fully-magnetized electron limits can be easy investigated from a fluid point of view, e.g. using EASYPLUME and DIMAGNO codes[10, 14]. By integrating the electron motion with ion motion or with magnetic invariants, fluid equations can be closed and solved to recover most physical phenomena of the far region. However, to explore the complex transition regime, for example the charged particles from magnetization to demagnetization in a propulsive magnetic nozzle, electron thermodynamics are hardly self-consistent in the near-collisionless plasma. Therefore, it is better approached with Particle-in-cell (PIC) codes due to the relief from electron dynamic assumptions.

Despite the simplicity of electron mobility problem in a fully kinetic PIC description on plasma expansion undergoes, there are certain technical difficulties in setting boundary conditions (BCs) since the actual situation outside the computational domain is initially unknown. In a plasma plume, most electrons are confined by the ambipolar electric field. Only the most energetic ones overcome this potential barrier and escape to infinity to neutralize the ion beam and maintain the current-free condition. The reflection of electrons by the electric potential occurs in the near and in the far region of the plume. When modeling only part of the plume, it is necessary to account for those electrons that leave the computational domain but will be reflected further downstream by the electric field, outside of the computational domain, and return to it. Otherwise, an inadequate open BC model would lead to electron depletion inside the domain and dramatically impact on the results. Referring to most plume electron-ion coupling and neutralization studies[4, 15-17], a current-free mode was typically implemented for the plasma source exit. Nevertheless, very few special procedures other than the potential Neumann condition and particle removal condition were found for open boundaries. Instead, they allowed the plasma to expand over reasonable durations while requiring the open system as large as possible to try to take more trapped electrons into consideration, as a result of which computational costs sharply increased and steady states were only partially obtained. Also it should be mentioned that in Ref. 16 modeling on near plume, an external BC based on conservation of energy was tentatively developed to overcome the numerical instability brought by reflection of electrons. To cover both near- and far-returning electrons within a finite simulation domain, we shall start a far-field plume expansion model with global BC consideration in terms of particles injection, reflection, and escape.

Generally the electron thermodynamic properties are of major concern within expansive plasma[8, 18]. Like in fluid descriptions, many used isothermal and polytropic sub-models to plot distributions of electron temperature, as well as of potential and density[14, 17, 19]. In theory the effective cooling coefficient $\gamma = 1$ corresponds to a constant electron temperature while $\gamma = 5/3$ represents an adiabatic process for monoatomic gases. However, no physical justification for these electron-cooling models exists in a collisionless expansion, where the equilibrium assumptions possibly fail in local and non-Maxwellian or anisotropic populations generate[20]. Thus to demonstrate the electron cooling process, kinetic models are required. Latest advances with kinetic models show that the electrons do cool down as they expand at a rate below adiabatic, and that trapped electron populations exist[21].

In this paper, a 2D full-PIC code, derived from Ref. 22, is first validated and benchmarked against several analytical and fluid cases. In order to avoid endless extension demand of the simulation domain and to overcome the expensive computation cost, finite planar dimensions in connection with the challenge of reaching global steady states motivate us to seek proper BCs for expanding particles and electric potential without numerical artifacts. Thereafter we use such in-house PIC code to explore physical details from unmagnetized electrons, like in the plume of a gridded ion thruster, to magnetized electrons, as in a magnetic nozzle, thus bracketing the transition regime of interest. Also, a sensitivity discussion of the plasma parameters and initial conditions is carried out. In what follows, we comment on the collisionless electron cooling mechanisms while correlate them to the AKILES kinetic results[21].

Section II describes the full-PIC simulation code with the highlight of fundamental boundary conditions for both electric field and plasma particles. Section III simulates an un-magnetized hypersonic plasma plume and correspondingly compares against fluid predictions. The collisionless electron cooling is then discussed. Section IV investigates the magnetic nozzle effect based on the Helicon plasma source. The full-PIC code illustrates the transition from fully magnetized electrons to unmagnetized electrons from a kinetic point of view.

## II. Simulation Model

We consider a slender collisionless plasma plume expansion into the surrounding vacuum within a two-dimensional planar geometry, which is symmetric with respect to the meridian plane $r = 0$. Any background pressure influences are excluded. It should be pointed out that we greatly lowers the requirement for computing sources by initializing the plume of radii of a few Debye lengths and selecting small but real proton to electron mass ration $m_i / m_e$=1836 (i.e. Hydrogen). Altogether it makes the simulation work feasible using one ordinary computer workstation.

### A. Full-PIC Code Description

Indeed, numerical investigations via full-PIC procedures are of a clear drawback of consuming enormous computation effort, which originates from the remarkable discrepancies between algorithmic time and space scales and dimensions of subjects studied. Basically according to the criteria of PIC procedure, a single cell size $\Delta x$ measures to one plasma Debye length $\lambda_{De0}$, and an advancing time-scale $\Delta t$ is taken no greater than $0.1\omega_{pe0}^{-1}$; if necessary, $\Delta t \leq 0.35\omega_{ce0}^{-1}$ should be taken into consideration to be capable to depict electrons gyro-motion. Moreover, in some explicit electromagnetic (EM) plasma simulations, the time step must also satisfy the Courant–Friedrichs–Lewy (CFL) condition $\Delta t \leq c\Delta x$ for a complete solver of the Maxwell's equations. Here coming to the mesothermal plasma plume expansion, typically $v_{te} >> v_{beam} >> v_{ti}$, we shall use an electrostatic (ES) model without constraining each time step to the light speed[15, 16, 20]. In this way the computing duration is largely depended on the ion plasma period and most electrons in the meantime are pacing forth and back between the ion beam front and somewhere downstream of the plume.

In the kinetic full-PIC model, highly mobile electrons are treated as an individual particle species same as the almost ballistic ions. The movements of all particles on the Cartesian grids are explicitly resolved by the Boris's scheme (as Eq. (1) with $\Delta t = t_{a+1} - t_a$), according to the Newton-Lorentz equations (as Eq. (2))[23, 24].

$$\begin{cases} \boldsymbol{x}_{a+1} = \boldsymbol{x}_a + \Delta t \cdot \boldsymbol{v}_{a+1/2} \\ \boldsymbol{v}_{a+1/2} = \boldsymbol{u}' + q'\boldsymbol{E}_a \end{cases}$$

$$\text{with } \boldsymbol{u}' = \boldsymbol{u} + (\boldsymbol{u} + \boldsymbol{u} \times \boldsymbol{h}) \times \boldsymbol{s},\ \boldsymbol{u} = \boldsymbol{v}_{a-1/2} + q'\boldsymbol{E}_a, \tag{1}$$

$$\boldsymbol{h} = q'\boldsymbol{B}_a,\ \boldsymbol{s} = \frac{2\boldsymbol{h}}{1+h^2},\ q' = \frac{q\Delta t}{2m}.$$

$$\begin{cases} m\dfrac{d\boldsymbol{v}}{dt} = q\left(\boldsymbol{E} + \boldsymbol{v} \times \boldsymbol{B}\right) \\ \dfrac{d\boldsymbol{x}}{dt} = \boldsymbol{v} \end{cases} \tag{2}$$

Within each electron-scaled time step, the electric charge is deposited onto its four neighboring grid nodes by the Ruyten's density-conserving shape factor $S(x_p, x_k)$[25] (which essentially reduces to bi-linearly relation in a planar cell). Then the number density is obtained

$$n_k = \sum_p w_p S(x_p, x_k) \tag{3}$$

where $x_k$, $x_p$ denote the position of a grid node and of a macro-particle, respectively, while $w_p$ is the specific weight of a macro-particle. We subsequently solve the self-consistent electrostatic field through the Dynamic Alternating Direction Implicit (DADI) algorithm based on the Poisson's equation[26], which portrays the local finite charge non-equilibrium, in return, motivating the differently charged particles to compensate it.

The computational domain together with applied magnetic field topology is sketched in Fig. 1, where the magnetic field distributes in parallel with plasma flow direction. The induced magnetic field is assumed negligible regarding this model. Two particle species of fully ionized plasma are considered here, i.e. single-charged ions and electrons.

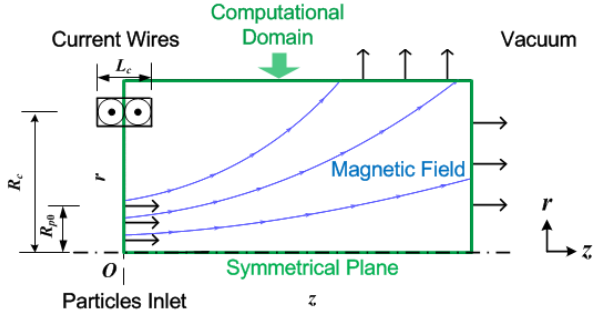


Figure 1. Simulation domain and magnetic field topology, for the simulations with a magnetized plasma.

Hereafter for convenience, subscripts $e$, $i$, will refer to a property evaluated for electrons and ions respectively, and 0 will refer to a property given at the initial site. The plasma efflux radius $R_{p0}$ will scale the axial distance $z$ and radial distance $r$ appearing in all sections. Again, all physical parameters of SI units are non-dimensional during the whole simulation (as Eq. (4)).

$$x=\frac{x_{(\mathrm{SI})}}{\lambda_{De0}},\ t=\frac{t_{(\mathrm{SI})}}{\omega_{pe0}^{-1}},\ q=\frac{q_{(\mathrm{SI})}}{e},\ v=\frac{v_{(\mathrm{SI})}}{v_{te0}},\ n=\frac{n_{(\mathrm{SI})}}{n_{e0}},\ T=\frac{T_{(\mathrm{SI})}}{T_{e0}},\ \Phi=\frac{e\Phi_{(\mathrm{SI})}}{k_B T_{e0}}. \tag{4}$$

## B. PIC Code Boundary Conditions

Figure 2 shows three main types of BCs related to the plasma expansion model, which are: 1) particles inlet (i.e. plasma source orifice) at the left-bottom of domain (enlarged in diagram to show details); 2) symmetric plane (SP) located at $r = 0$; 3) outer boundaries (OBs) at the left, up, and right sides, representing the outside vacuum space. As for the electric field, like most did before, we set the reference potential constant as zero at the inlet; meanwhile assume the Neumann condition of zero normal gradient on the three downstream borders. Note that applying Neumann conditions to the external boundary has an influence in the neighborhood of the boundary conditions, which could partly divert plasma simulating distributions nearby.

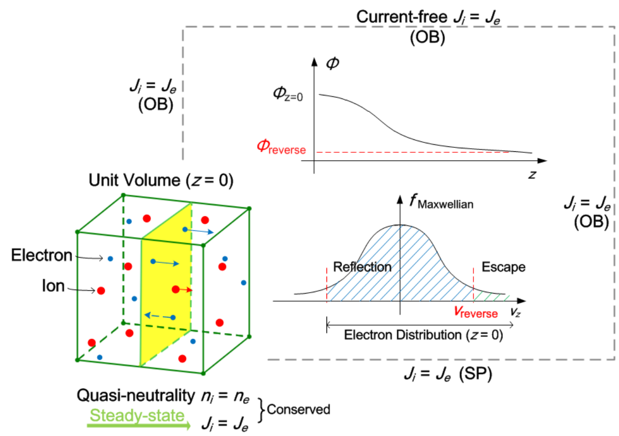

Figure 2. Boundary conditions of the plasma expansion model. Both quasi-neutral and current-free conditions are conserved in a unit volume at the inlet.

The major difference of BCs among PIC codes exists in management of numerical macro-particles, especially regarding the mobile electrons. It is of great difficulty in setting vacuum boundaries for them since the number of electrons streaming back to the source is unknown a priori, and in some cases, their reflection points probably locate outside the computational domain. As illustrated in the introduction section, ions expanding crossing those boundaries are generally beyond simulation and immediately neutralized by the most energetic fraction of electrons, forming a current-free beam.

Considering the single-peaked plasma plume in a far-thruster region, we in principle expect both quasi-neutrality and current-free state to be conserved within the plasma source. However, in fact, it is complex to satisfy such two conditions simultaneously only through the particles emission. Since the velocity distributions of electrons and ions are quite different therein. Supposing all ions are injected to a simple mono-energetic distribution[6], the sum of emitted and reflected electrons then should altogether form a net current of absolute value equivalent to that single-directed ion current. While it is far from the final steady state, we can hardly estimate the exact number of electrons returning by or passing through the potential barrier in an expanding plume. Hence it is nearly possible to implement the specific emission electron-current at the very beginning of PIC simulation.

Strictly speaking, it should be viewed as an integral problem of BC settings for electrons' access. Contrasting to most others' work, our solution focus on two aspects that, on one hand, we force the quasi-neutrality at particles emission in steady of conventional current condition; and on the other hand, we instantly return those electrons crossing OBs but with relatively lower energy based on the global current-free condition. In this way we make the OBs act like filters, through which only a few high-energized electrons are allowed to escape towards infinity (see Fig. 2). One should also note that no current ambipolarity condition has to be constrained everywhere throughout the whole simulation domain, thus a possible distribution of the local net plasma current exists. Hopefully, in the steady state, we shall achieve a dynamically balanced emission current of electrons and ions. At the same time, a sufficient population of trapped electrons will be rationally demonstrated by using our BCs.

In terms of the emission process, we assume a uniform plasma radial density profile within the range of $0 \le r \le R_{p0}$. The thermal temperature of ion source is considered ignorable to that of electrons. The macro speed of ions is scaled by the Mach number $M = v_i / c_s$, where $c_s$ represents the acoustic speed. Also, the ion radial velocity component is given related to the plume original divergence angle $\alpha_0$[12].

$$v_{i,r0} = \frac{M_0 c_{s0} r}{R_{p0}} \cdot \tan\alpha_0 \tag{5}$$

The thermal and stationary electrons generally distribute Maxwellian in the upstream source; to be specific, free molecular effusion effects should be considered for their emission[15]. For example along the $z$-coordinate, we sample the electrons from an individual Maxwellian function with a macroscopic drift velocity equivalent to the bulk ion velocity.

So far, we have illustrated the major concern with source, lateral and downstream boundaries in plasma plume expansion. Before stepping into the complex multi-dimensional simulation, we shall investigate these BC effects as well as to test the coding procedures. Again, it should be mentioned that we are going to present results from like 80% of the computational domain to leave out the border effect.

### C. Investigation of Boundary Condition Effects

We preliminary assume an infinite plasma plume with zero divergence to validate the aforementioned boundary conditions. Some simplifications from what Fig. 1 shows are: 1) a sonic plasma flows within an extremely narrow domain, which turns out to be 1D situation and only $z$-directional variations are concerned; 2) two periodic boundaries are applied in the lateral direction; 3) no magnetic field exists in this model. Table 1 summarizes the relevant simulation parameters. Basic properties of plasma, like $n_{e0}$ and $T_{e0}$, are chosen as the same as those used in the following 2D unmagnetized plume simulation (see Section III).

Table 1. Simulation parameters in test cases.

| Number of grids ($z \times r$) | Number of macro-particles (e.g. ions) | Time step | Macro-particle weight | Injection plasma radius |
|---|---|---|---|---|
| 500 × 5 | > 90 thousand | $0.05\ \omega_{pe0}^{-1}$ | 60 | $5\ \lambda_{De0}$ |
| Initial ion Mach number | Initial plume divergence angle | Electron temperature (reference) | Plasma density (reference) | Debye length (reference) |
| 1 | 0° | 3 eV | $1\times10^{18}$ m$^{-3}$ | $1.3\times10^{-5}$ m |

Note that we are testing two sets of BCs for particles emission from the left and their escape from the right: 1) injecting electrons and ions based on the quasi-neutral condition and keeping the current-free condition at the open boundary (as illustrated in the above subsection); 2) injecting electrons and ions based on the current-free condition and allowing them to leave simulation domain freely (as previously used in most studies).

Figure 3 shows that a relatively stable transition process performs under the quasi-neutral emission and current-free filtering mode as we expected. The simulation steady state roughly arrives after $t = 3000\omega_{pe0}^{-1}$ and a plasma flow of overall uniform density as well as quasi-neutral electricity gradually forms. Compared with this, however, we observe a notable potential jump near the plasma source orifice when implementing the BCs of current-free emission and wide-open downstream (see Fig. 3(c)). It indicates a large imbalance of charge at the emission plane, and also leads to impossibility of an overall steady state for finite simulating dimensions. Therefore, it is quite important to have the correct BCs to avoid artificial effects.

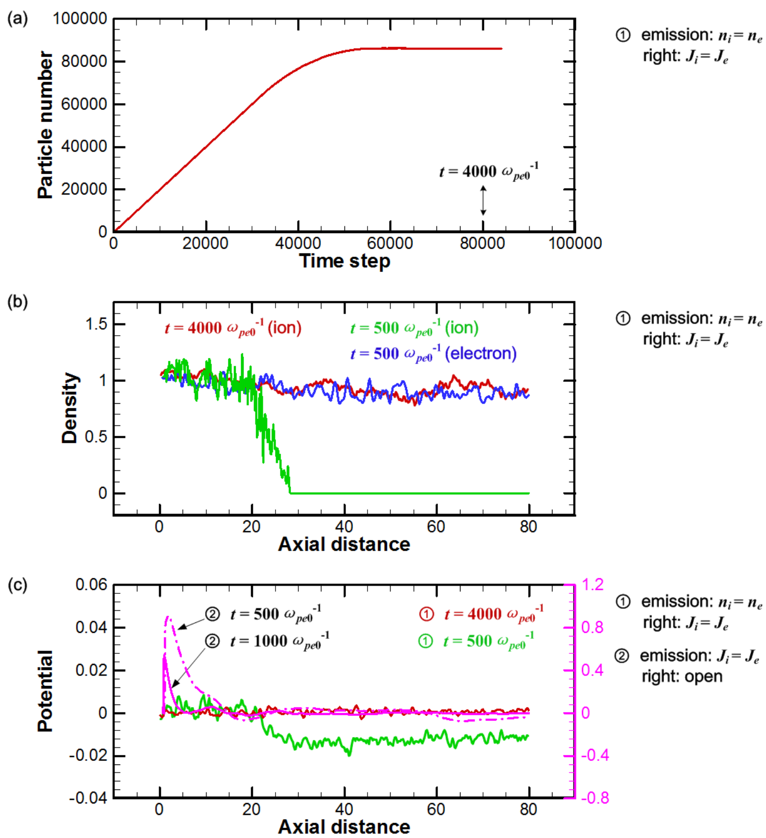


Figure 3. Plume evolution with different boundary settings. (a) Ion particle number, (b) Plasma density, (c) Electric potential. Curves of (b) and (c) are averaged along the *r* direction respectively.

## III. Unmagnetized Plume Expansion

### A. Simulation Set

The pre-described 2D full-PIC code is carried out to simulate an unmagnetized plasma plume expanding into the vacuum. To compare this work against reported fluid studies[12, 14], we choose a set of varying cases with the same initial conditions as those used before, such as the ion Mach number and plume divergence angle (listed in Table 2). The computational electron temperature and density, as well as beam velocity is characterized referring to the existing plasma thrusters, e.g. the Gridded Ion Thruster and the Hall Effect Thruster[27].

Table 2. Simulation parameters in the 2D unmagnetized plume expansion.

| Number of grids ($z \times r$) | Number of macro-particles (e.g. ions) | Time step | Macro-particle weight | Injection plasma radius |
|---|---|---|---|---|
| 300 × 50 | > 30 thousand | $0.1\omega_{pe0}^{-1}$ | 80 | $10\lambda_{De0}$ |
| Initial ion Mach number | Initial plume divergence angle | Electron temperature (reference) | Plasma density (reference) | Debye length (reference) |
| 5 & 15 | 0° & 10° | 3 eV | $1\times10^{18}$ m$^{-3}$ | $1.3\times10^{-5}$ m |

### B. Steady State Results

Computationally it is necessary to average data of properties over long enough duration to eliminate numerical instabilities. In our code, it is done within the last 20% of time steps after reaching the steady state. As seen in Fig. 4, for example, the total ion number roughly stabilizes after $t = 600\omega_{pe0}^{-1}$. So we can count the net charge number passing through the inlet during $t = (1000 - 1500)\ \omega_{pe0}^{-1}$ to examine the global current-free condition that should be served together with the quasi-neutrality. As in the case of $M_0 = 15$ and $\alpha_0 = 10°$, it is clear to see a fluctuating number of about $\pm 10$ macro-charges per time-step in normalization, which corresponds to a relatively small net current of ± $7.1\times10^{-5}$ C/s (using $J_{inlet} = \pm10ew_p/\Delta t$) applied in the particles stable emission. In other words, the global current-free plasma condition has been approximately realized at the entrance.

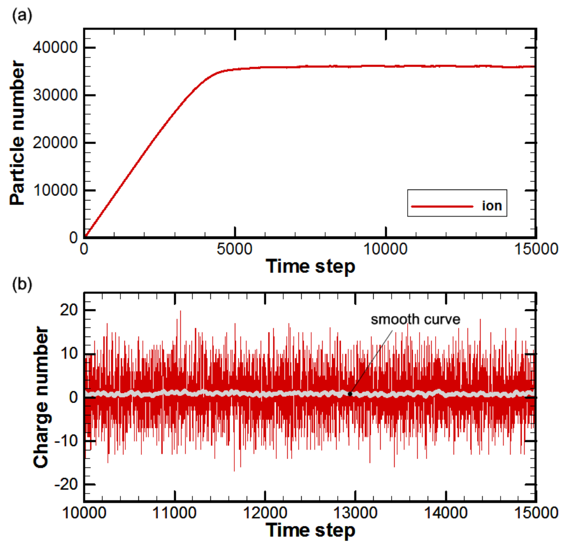


Figure 4. Number fluctuations during the steady state. (a) Ion particle number, (b) Moving charge number at the inlet. $M_0 = 15$ and $\alpha_0 = 10°$.

The results of plasma density are plotted varying with different initial conditions (see Fig. 5). An expansion fan region is clearly observed by the iso-density lines in each case. The discrepancy of number density between ion and electron only appears notable along the plasma edge within (2 - 5) $R_{p0}$ distance from the inlet plane, which might be viewed as the non-neutral transition layer from the inside plasma to outside vacuum space. Compared with previous fluid and kinetic plasma distributions[12], most characteristics are quite similar. To scale the axial range of undisturbed beam core in the cases of zero initial divergence (see Fig. 5(a)(c)), the slope of Mach line is calculated as $k_M = \tan\theta$, where $\theta = \sin^{-1}(1/M)$. Hence, in theory, Mach line should cross the symmetric plane at $z \approx 15$ for $M_0 = 15$ and at $z \approx 4.9$ for $M_0 = 5$. Whereas in our simulation, these points both slightly shift left, suggesting a reduced Mach number that is actually applied at the very beginning. Moreover, the paraxial density comparisons are also carried out using the PIC solution and EASYPLUME equation[14]. Shown by Fig. 6, a good agreement between such two methods is observed. The expansion density of a higher Mach number seems even more adaptive for the fluid description.

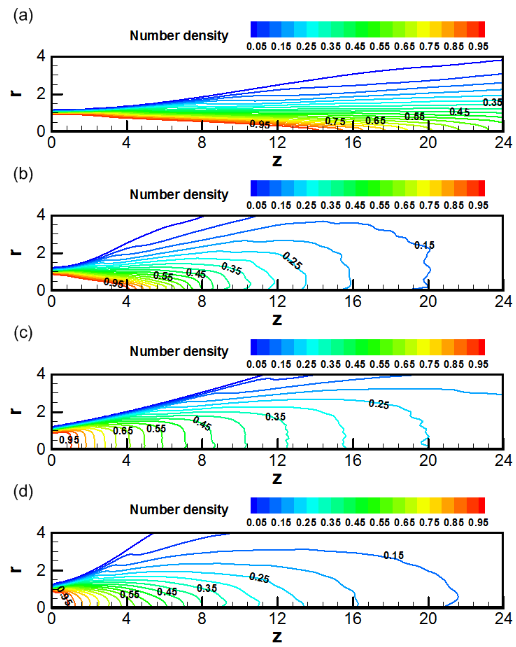


Figure 5. Contour plots of ion number density. (a) $M_0 = 15$ and $\alpha_0 = 0°$, (b) $M_0 = 5$ and $\alpha_0 = 0°$, (c) $M_0 = 15$ and $\alpha_0 = 10°$, (d) $M_0 = 5$ and $\alpha_0 = 10°$.

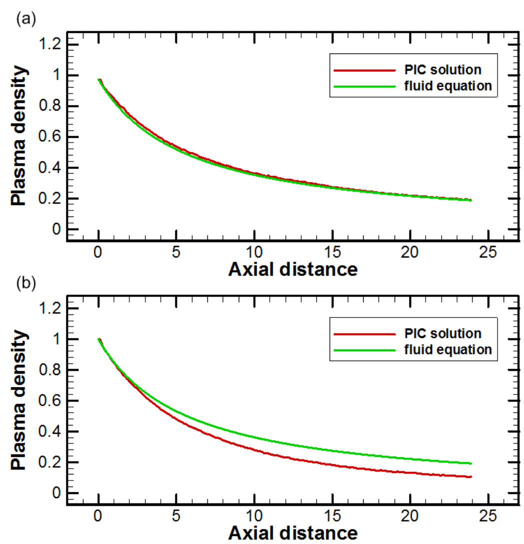


Figure 6. Paraxial plasma density comparisons. (a) $M_0 = 15$ and $\alpha_0 = 10°$, (b) $M_0 = 5$ and $\alpha_0 = 10°$.

### C. Collisionless Electron Cooling

We investigate the collisionless electron cooling characteristics from varying relations of electric potential $\Phi$ and electron density $n_e$ using this kinetic full-PIC code. In the paraxial region of an expanding plasma, the calculated electric potential monotonically drops to $(1 - 2)\ T_{e0}$ within the axial distance of 20 $R_{p0}$ (see Fig. 7). Also during this process, we notice that the PIC solution matches well with the isothermal fluid model ($\gamma = 1$) under various circumstances, except in Fig. 7(a) the PIC simulated potential appears closer to the polytropic law of $\gamma$ slightly larger than 1.2. However, in most cases the electron temperature could be roughly assumed constant within the central part of a hypersonic plume.

Considering the plasma divergence, for example as depicted in Fig. 8, the electron thermodynamics are regionally changing. We compare the corresponding electron cooling rates varying with expansion by plotting the electric potential drops along 50%, 70%, 90% plasma density lines, respectively. Overall, an obvious trend can be observed that the electrons undergo a faster cooling in outer part of the plasma plume with the factor $\gamma$ growing up to 2, even slightly larger than an adiabatic case. While comparing among different potential curves in Fig. 8(b), we find such effective cooling rate diminishing inward the plasma plume, suggesting a waning process of the collisionless electron cooling.

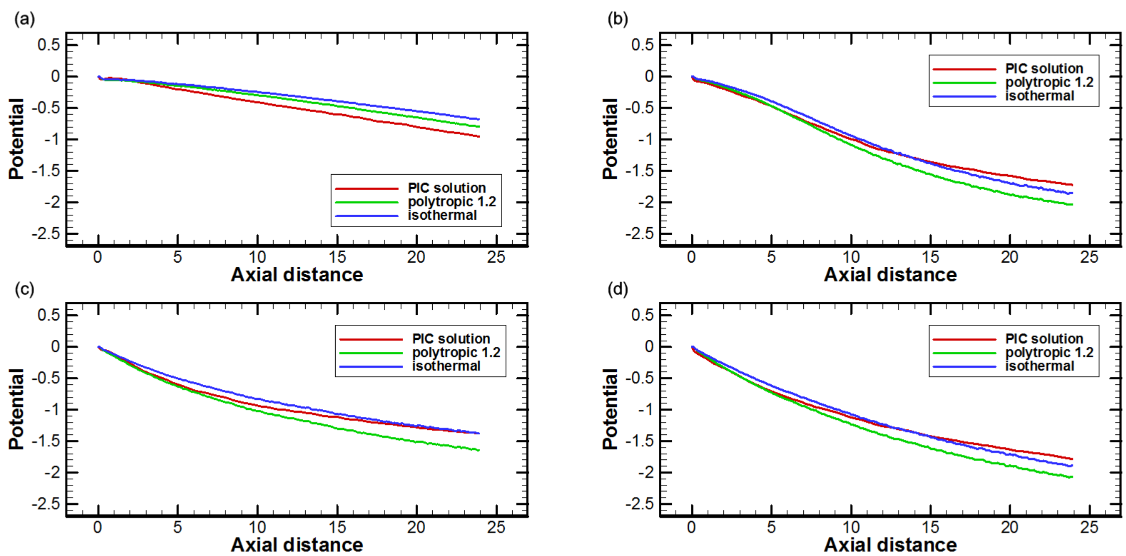


Figure 7. Paraxial electric potential variations. (a) $M_0$ = 15 and $\alpha_0$ = 0°, (b) $M_0$ = 5 and $\alpha_0$ = 0°, (c) $M_0$ = 15 and $\alpha_0$ = 10°, (d) $M_0$ = 5 and $\alpha_0$ = 10°.

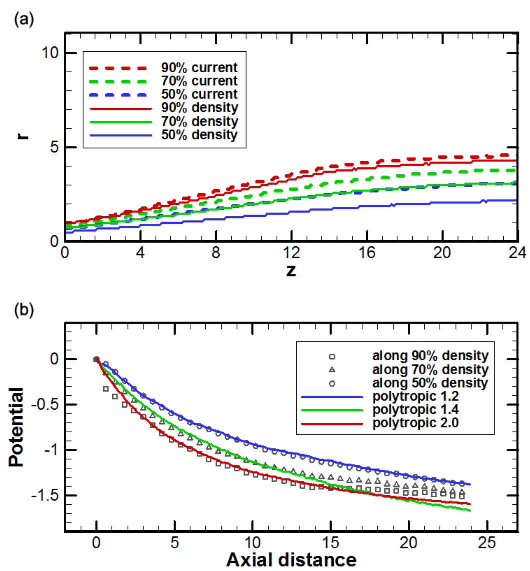


Figure 8. Polytropic relation along the density lines. (a) 50%, 70%, 90% plasma current and density lines, (b) Electric potential along the density lines. $M_0$ = 15 and $\alpha_0$ = 10°.

## IV. Plasma Magnetic Nozzle

### A. Simulation Set

Changing the magnetic background environment for a plasma plume can greatly impact on its expansion tendency thereby generates a plasma magnetic nozzle (MN). To investigate this, we apply a set of solenoid coils of radius $R_c = 3R_{p0}$, and subsequently produces different magnetic field strengths by simply adjusting currents (see Fig. 9). The intensity of applied magnetic field is characterized by the normalized ion gyration frequency (as Eq. (6)) in our comparative full-PIC simulation cases. As illustrated in Fig. 1, the strongest magnetic field exists at the throat, where the plasma injection plane locates as well.

Table 3 includes major parameters in terms of the MN simulation. A relative hot-electron and cold-ion plasma source is considered as for the Helicon type thrusters[10]. Again, an initial radial-uniform density profile as well as no initial divergence angle is assumed in this plasma plume model.

$$\Omega_{i0} = \frac{q_i B_0 R_{p0}}{m_i v_{i,r0}} \tag{6}$$

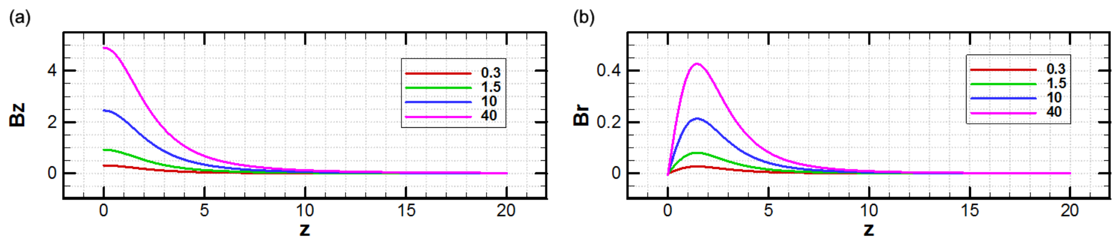


Figure 9. Varying magnetic conditions for $\Omega_{i0}$ = 0.3, 1.5, 10, 40.

Table 3. Simulation parameters in the 2D magnetic nozzle.

| Number of grids ($z \times r$) | Number of macro-particles (e.g. ions) | Time step | Macro-particle weight | Injection plasma radius |
|---|---|---|---|---|
| 200 × 120 | > 300 thousand | $0.1\omega_{pe0}^{-1}$ | 40 | $10\lambda_{De0}$ |
| Initial ion Mach number | Initial plume divergence angle | Electron temperature (reference) | Plasma density (reference) | Debye length (reference) |
| 1 | 0° | 20 eV | $7\times10^{18}$ m$^{-3}$ | $1.3\times10^{-5}$ m |

**B. Steady State Results**

Figure 10 provides some convergence results without magnetic field as the reference case for MN study. What can be intuitively seen therein is a freely expanding plume of electrons and ions streamlines approximately coincide with each other. The electric potential drops 3.56 $T_{e0}$ at maximum, which corresponds to a self-consistent acceleration of ions and purely electric confinement of electrons. The plasma density lines plotted in Fig. 10(a) represent some certain portions of ion mass flow. Again, observe that there is a blank area near the left vacuum boundary in the plasma density distribution, which we consider as the result apparently affected by the von Neumann BC on the electric potential.

The magnetic nozzle influences on plasma characteristics are partially demonstrated in Fig. 11, focusing on the ion density and axial velocity distributions. We can obviously see an increasing channeling of the plasma plume, in particular near the magnetic throat. At the same time, the ion plasma structure seems to split into two parts that one bulk part containing 90% plume flow while another tiny and less-disturbed part wrapping around the former within the axial distance of several initial plasma radii. In all cases, the ion axial velocity increases downstream; however, very little ion acceleration is seen as the magnetic field gradually enhanced.

The ion streamline separation, which is central to plasma detachment, was already studied in Ref. 28. Here by this full-PIC work, what would be interesting to give is the transition of electron streamlines, of which the distribution trend should concurrently vary with the magnetic field, e.g. showing coincidence when the field is strong and separation when it becomes weak. Indeed, we observe the fully magnetization duration of electrons is gradually prolonged with $\Omega_{i0}$ increasing from 0.3 to 10, from the spread of electron current lines (see Fig. 12). Also for the sake of contrast, we portray the electron velocity streamlines over the magnetic field lines as well as over the ion streamlines in each case. In order to find specific position of electron-field separation, seen Fig. 12(a) for example, we roughly position the detachment points at around $5R_{p0}$ after plasma emission; however, as more and more ions are initially magnetized, the electrons transition site from fully magnetization to unmagnetization is remarkably moving farther downstream, and probably after several times of translation of their gyro-centers.

In theory the process of electrons demagnetization is happening under the competition among the magnetic guidance, electric linkage to ions, and inertia of their own. Also, the detachment of electrons and ions should interrelate with each other both in time and in space owing to the strong coupling ambipolar field. According to the comparative views on particle streamlines, a vast majority of non- and low-magnetized ions step straight through the magnetic field therefore critically affects the plume divergence and electrons escape from the guiding magnetic field. Another observation among the results is the trajectory discrepancy between electrons and ions. It is noticeable when fewer ions are magnetized, thus probably indicating the local plasma current formation in terms of the large charge separation. However, it broadly vanishes as the ion magnetization degree increases, as a result of which both species of particles break with the weakening magnetic field mostly from the inner side.

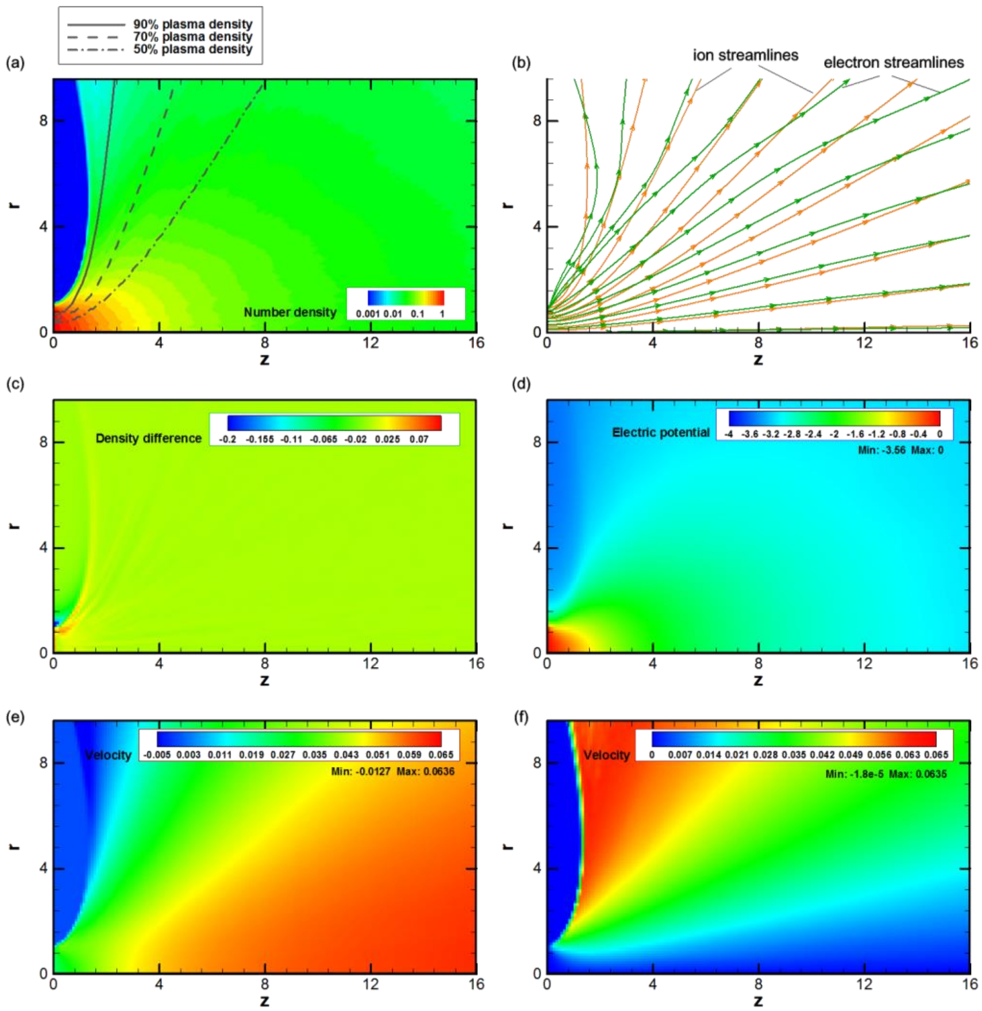


Figure 10. Simulation results for a reference case without magnetic field. (a) Ion number density contour along with 50%, 70%, 90% density lines, (b) Ion and electron velocity streamlines, (c) Density difference between ion and electron, (d) Electric potential, (e) Ion axial velocity, (f) Ion radial velocity.

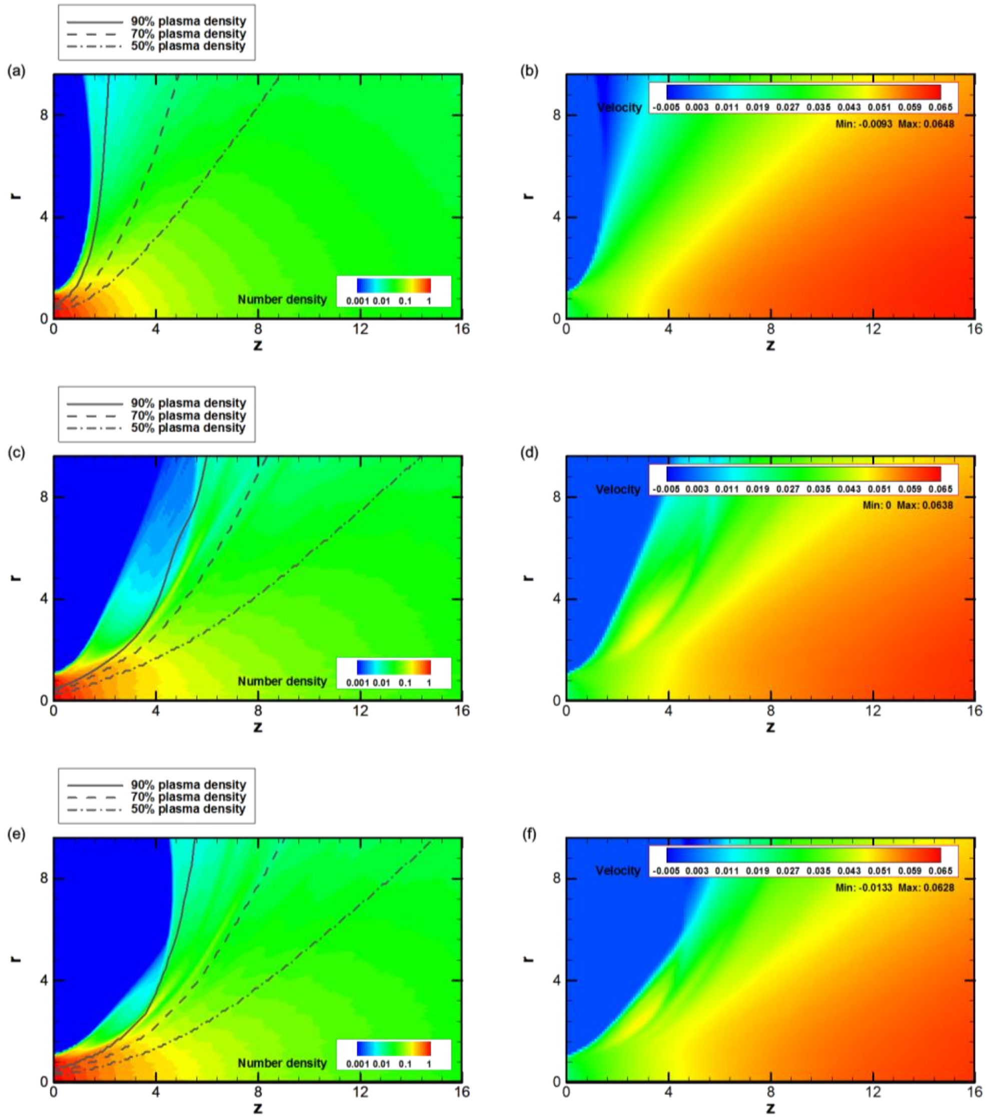


Figure 11. Contour plots of ion density along with 50%, 70%, 90% density lines (Left) and ion axial velocity (Right). (a)(b) $\Omega_{i0} = 0.3$, (c)(d) $\Omega_{i0} = 1.5$, (e)(f) $\Omega_{i0} = 10$.

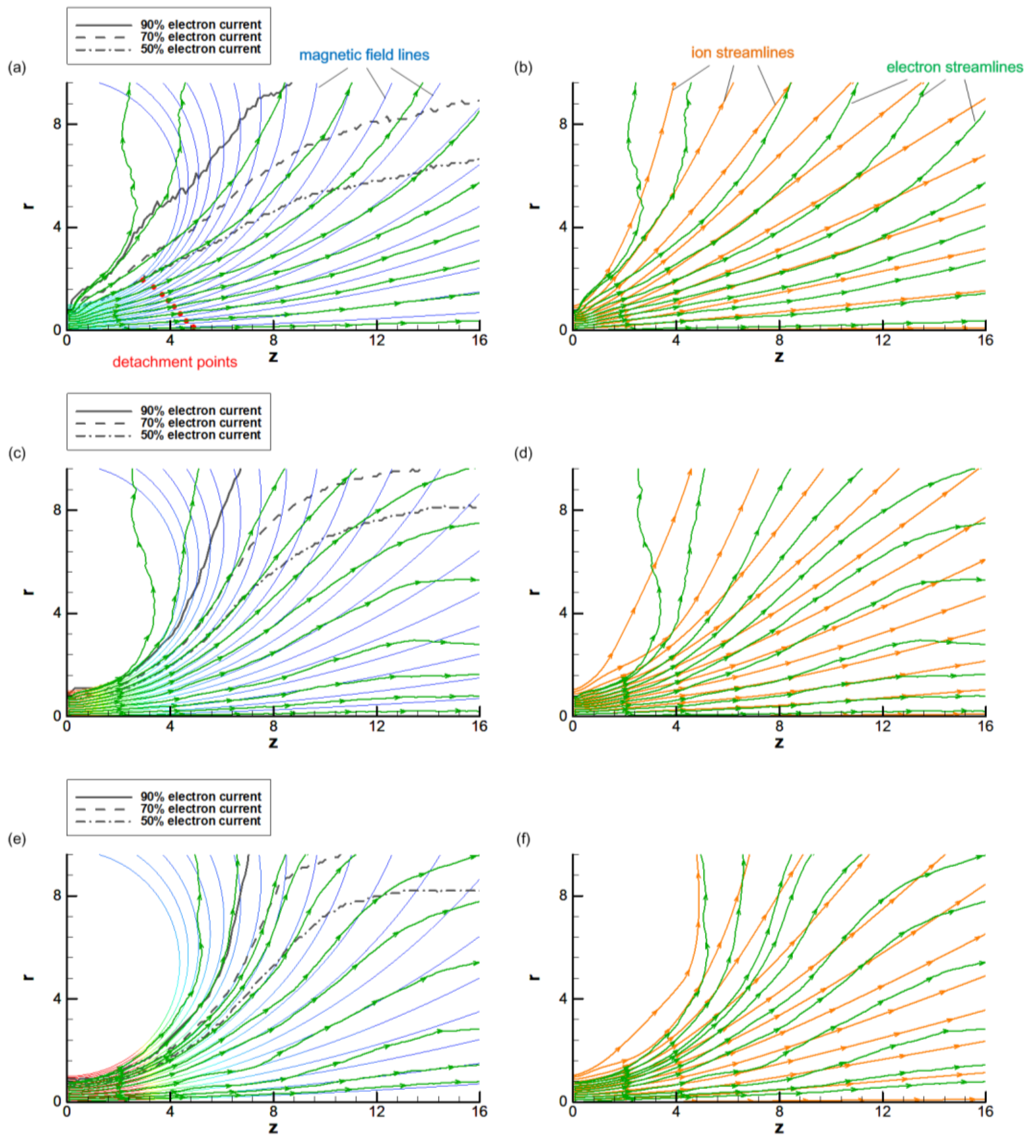


Figure 12. Particle streamlines and electron current lines spreading over magnetic field lines. (a)(b) $\Omega_{i0}$ = 0.3, (c)(d) $\Omega_{i0}$ = 1.5, (e)(f) $\Omega_{i0}$ = 10.

## V. Conclusions

In this paper, the planar, electrostatic, full-PIC simulation of a 2D, slender, collisionless plasma plume expansion into vacuum has been carried out.

In order to overcome numerical artifacts brought by boundary conditions of a finite computational domain, our work first demonstrates and validates several proper choices for both electric potential and macro-particles boundary conditions. These settings originate from a global consideration regarding the plasma source property as well as the trapped electrons in a far-thruster region, which in principle two conditions of quasi-neutrality and current-free should be simultaneously conserved at the particles emission plane.

Thereafter using the full-PIC code, we have comparatively studied the transition regime from unmagnetized electrons, as in the plume of a gridded ion thruster, to magnetized electrons, as in a magnetic nozzle. For each simulation case, the steady state is globally achieved and hence benchmarked against reported fluid codes, like EASYPLUME and DIMAGNO. We have observed a good agreement between the full-PIC solution and the fluid equation as a function of the initial ion Mach number and initial plume divergence angle. Regarding the collisionless electron cooling effect, the widely used isothermal assumption almost stands within the central part of a hypersonic plume; whereas for the outward plasma plume, the electrons cool as the polytropic relation of a larger rate, even slightly faster than an adiabatic process. Moreover, we have seen an obvious increasing channeling influence inside a plasma magnetic nozzle. As the magnetic field enhanced, very little ion axial acceleration has been found; however a back flow of ion plume gradually grows suggesting us to achieve an optimal magnetic condition at some low ion magnetization degree. The last but interesting thing in this work is that we have demonstrated the demagnetization process of fully magnetized electrons in terms of the applied magnetic field lines as well as the ion streamlines. The magnetization duration of electrons is constantly prolonged with an increasing $\Omega_{i0}$, thereby they roughly detach farther downstream, after probably translating among several gyro-centers. It is critical to see a vast majority of non- and low-magnetized ions stepping straight through the magnetic field since it notably influences on the plume divergence and electrons escape from the magnetic confinement. The trajectory differs large between electrons and ions in these cases, indicating the possible formation of local plasma currents. However as more ions get magnetized, two species of particles almost coincide with each other and leave from the weakening magnetic nozzle mostly from its inner side.

Regarding further work, the full-PIC simulation code may be extended including more influential aspects, like the background pressure and relevant collisions. The type of ion distribution upstream may be imposed in terms of its thermal temperature. In addition, a 2D axisymmetric geometry could compare against this planar one in order to discuss on the cylindrical effects.

## Acknowledgments

Min Li's work has been supported by the Doctor's internship fund of Beihang University, China. Mario Merino and Eduardo Ahedo's work has been supported by the Spanish R&D National Plan under grant number ESP2016-75887-P. Additionally support has been provided by the Fundamental Research Program (No. JCKY2017601C), China.

## References

[1]Jahn, R. G., *Physics of Electric Propulsion*, McGraw-Hill, New York, 1968.

[2]Schoenberg, K. F., Gerwin, R. A., Moses, R. W, Jr., Scheuer, J. T., and Wagner, H. P., "Magnetohydrodynamic Flow Physics of Magnetically Nozzled Plasma Accelerators with Applications to Advanced Manufacturing," *Physics of Plasmas*, Vol. 5, No. 5, 1998, pp. 2090-2104.

[3]Liemohn, M. W., and Khazanov, G. V., "Collisionless Plasma Modeling in an Arbitrary Potential Energy Distribution," *Physics of Plasmas*, Vol. 5, No. 3, 1998, pp. 580-589.

[4]Denavit, J., "Collisionless Plasma Expansion into a Vacuum," *The Physics of Fluids*, Vol. 22, No. 7, 1979, pp. 1384-1392.

[5]Arefiev, A. V., and Breizman B. N., "Ambipolar Acceleration of Ions in a Magnetic Nozzle," *Physics of Plasmas*, Vol. 15, 2008, pp. 042109.

[6]Martinez-Sanchez, M., Navarro-cavallé, J., and Ahedo, E., "Electron Cooling and Finite Potential Drop in a Magnetized Plasma Expansion," *Physics of Plasmas*, Vol. 22, No. 5, 2015, pp. 119-134.

[7]Vayner, B., "Cooling Electrons in Far Field of Plume Plasma," *14th Spacecraft Charging Technology Conference*, Noordwijk, The Netherlands, 2016.

[8]Little, J. M., and Choueiri, E. Y., "Electron Cooling in a Magnetically Expanding Plasma," *Physical Review Letters*, Vol. 117, 2016, pp. 225003.

[9]Hu, Y., and Wang, J., "Fully Kinetic Simulations of Collisionless, Mesothermal Plasma Emission: Macroscopic Plume Structure and Microscopic Electron Characteristics," *Physics of Plasmas*, Vol. 24, No.3, 2017, pp. 033510.

[10]Ahedo, E., and Merino, M., "Two-dimensional Supersonic Plasma Acceleration in a Magnetic Nozzle," *Physics of Plasmas*, Vol. 17, No.7, 2010, pp. 073501.

[11]Merino, M., and Ahedo, E., "Contactless Steering of A Plasma Jet with a 3D Magnetic Nozzle," *Plasma Sources Science and Technology*, Vol. 26, 2017, pp. 095001.

[12]Cichocki, F., Merino, M., Ahedo, E., Hu, Y., and Wang, J., "Fluid vs PIC Modeling of a Plasma Plume Expansion," *34th International Electric Propulsion Conference,* Hyoto-Kobe, Japan, July 4-10, 2015, IEPC-420.

[13]Ahedo, E., and Merino, M., "On Plasma Detachment in Propulsive Magnetic Nozzle," *Physics of Plasmas*, Vol. 18, 2011, pp. 053504.

[14]Merino, M., Cichocki, F., and Ahedo, E., "A Collisionless Plasma Thruster Plume Expansion Model," *Plasma Sources Science and Technology*, Vol. 24, No. 3, 2015, pp. 035006.

[15]Wang, J., Chang, O., and Cao, Y., "Electron–Ion Coupling in Mesothermal Plasma Beam Emission: Full Particle PIC Simulations," *IEEE Transactions on Plasma Science*, Vol. 40, No. 2, 2012, pp. 230-236.

[16]Brieda, L., and Wang, J., "Modeling of Ion Thruster Beam Neutralization Using a Fully Kinetic ES-PIC Code", *41st AIAA/ASME/SAE/ASEE Joint Propulsion Conference & Exhibit*, Tucson, Arizona, July 10-13, 2005, AIAA-4045.

[17]Pfeiffer, M., Copplestone, S., Binder, T., Fasoulas, S., and Munz, C. D., "Comparison of Plasma Plume Expansion Simulations Using Fully Kinetic Electron Treatment and Electron Fluid Models," *30th International Symposium on Rarefied Gas Dynamics*, *AIP Conference Proceedings*, Vol. 1786, 2016, pp. 130005.

[18]Lafleur, T., Cannat, F., Jarige, J., Elias, P. Q., and Packan, D., "Electron Dynamics and Ion Acceleration in Expanding-plasma Thrusters," *Plasma Sources Science and Technology*, Vol. 24, No. 6, 2015, pp. 065013.

[19]Merino, M., and Ahedo, E., "Influence of Electron and Ion Thermodynamics on the Magnetic Nozzle Plasma Expansion," *IEEE Transactions on Plasma Science*, Vol. 43, No. 1, 2015, pp. 244-251.

[20]Hu, Y., and Wang, J., "Electron Properties in Collisionless Mesothermal Plasma Expansion: Fully Kinetic Simulations," *IEEE Transactions on Plasma Science*, Vol. 43, No. 9, 2015, pp. 2832-2838.

[21]Merino, M., Fajardo, P, and Ahedo, E., "Collisionless Electron Cooling in Unmagnetized Plasma Thruster Plumes," *52nd AIAA/ASME/SAE/ASEE Joint Propulsion Conference*, *Propulsion and Energy Forum*, Salt Lake City, UT, July 25-27, 2016, AIAA-5037.

[22]Li, M., Tang, H. B., Ren, J. X., and York, T. M., "Modeling of Plasma Processes in the Slowly Diverging Magnetic Fields at the Exit of an Applied-field Magnetoplasmadynamic Thruster," *Physics of Plasmas*, Vol. 20, No.10, 2013, pp. 063501.

[23]Birdsall, C. K., and Langdon, A. B., *Plasma Physics via Computer Simulation*, Hilger, New York, 1991.

[24]Boris, J. P., "Relativistic Plasma Simulation-optimization of a Hybrid Code," *Proceedings of the 4th Conference on Numerical Simulation of Plasmas*, Naval Res. Lab., Washington, D.C. 1970, pp. 3–67.

[25]Ruyten, W. M., "Density-conserving Shape Factors for Particle Simulations in Cylindrical and Spherical Coordinates," *Journal of Computational Physics*, Vol. 105, 1993, pp. 224-232.

[26]Hewett, D., Larson, W., and Doss, S., "Solution of Simultaneous Particle Differential Equations Using Dynamic ADI: Solution of the Streamline Darwin Field Equations," *Journal of Computational Physics*, Vol. 101, 1992, pp. 11-24.

[27]Cichocki, F., Merino, M., and Ahedo, E., "Modeling and Simulation of EP Plasma Plume Expansion into Vacuum", *50th AIAA/ASME/SAE/ASEE Joint Propulsion Conference*, Cleveland, OH, July 28-30, 2014, AIAA-3828.

[28]Merino, M., and Ahedo, E., "Plasma Detachment in a Propulsive Magnetic Nozzle via Ion Demagnetization", *Plasma Sources Science and Technology* Vol. 23, 2014, pp. 032001.